LA-UR-99-2595

Approved for public release; distribution is unlimited.

Title: Flow visualizations and measurements of the mixing evolution of a shock-accelerated gas curtain

Author(s): Katherine Prestridge, Peter Vorobieff, Paul Rightley, Robert Benjamin

Submitted to: International Symposium on Shock Waves (ISSW22)
London, England
19-23 July 1999

Los Alamos
NATIONAL LABORATORY

DISCLAIMER

Flow visualizations and measurements of the mixing evolution of a shock-accelerated gas curtain

K. Prestridge, P.V. Vorobieff, P.M. Rightley, R.F. Benjamin

Dynamic Experimentation Division, Los Alamos National Laboratory, Los Alamos NM 87545, USA

Abstract: We describe a highly-detailed experimental charaterization of the impulsively driven Rayleigh-Taylor instability, called the Richtmyer-Meshkov instability Meshkov (1969). This instability is produced by flowing a diffuse, vertical curtain of heavy gas (SF_6) into the test section of an air-filled horizontally oriented shock tube. The instability evolves after the passage of a Mach 1.2 shock past the curtain, and the development of the curtain is visualized by seeding the SF_6 with small ($d \approx 0.5\mu$m) glycol droplets using a modified theatrical fog generator. Because the event lasts only 1 ms and the initial conditions vary from test to test, rapid and complete data acquisition is required in order to characterize the initial and dynamic conditions for each experimental shot. Through the use of a custom-built pulsed Nd:YAG laser, we are able to image the flowfield at seven different times. We acquire a double-pulsed image of the flow with the use of a second pulsed Nd:YAG, which is used to determine the instantaneous velocity field using Particle Image Velocimetry (PIV). During a single experiment, high resolution images of the initial conditions and dynamic conditions are acquired using three CCD cameras. Issues of the fidelity of the flow seeding technique and the reliability of the PIV technique will be addressed. We have successfully provided interesting data through analysis of the images alone (Rightley et al. (1999), Vorobieff et al. (1998), Rightley et al. (1997)), and we are hoping that PIV information will be able to add further physical insight to the evolution of the RM instability and the transition to turbulence.

Key words: Richtmyer-Meshkov instability, PIV, Mixing

1. Introduction

The Richtmyer-Meshkov (RM) instability, the impulsively driven analog of the Rayleigh-Taylor instability, is studied through the use of high-resolution imaging and Particle Image Velocimetry (PIV). The goal of this set of experiments is to provide quantitative information about the mixing transition and statistical properties of the instability to allow a better understanding of the RM instability as well as to validate hydrodynamic simulations.

An extensive review of early RM experiments is contained in Rightley et al. (1999). The present set of experiments is designed to study the RM instability by injecting a vertical curtain of heavy gas (SF_6) into the ambient air of a horizontal shock tube and triggering the instability at the interfaces of the gas curtain using a Mach 1.2 normal shock. Early gas curtain experiments used a light sheet to illuminate the SF_6 gas curtain (Jacobs et al. (1993), Budzinski et al. (1994)), however, the temporal resolution was limited to at most two dynamic exposures per event. Recent experiments have improved the spatial and temporal resolution by using tracer particles to track the SF_6 and a multi-framing camera to increase the temporal resolution to up to 32 frames per event (Rightley et al. (1999), Rightley et al. (1997)).

The current experiments have improved both the spatial and temporal resolution through the use of pulsed Nd:YAG lasers, more uniform light sheets, and multiple multi-exposure cameras. This work focuses on increased resolution of the dynamic images with simultaneous velocity field measurements. This article will describe the instrumentation being used to acquire new information about the RM instability, as well as preliminary results of the Particle Image Velocimetry (PIV).

2. Shock-tube facility

The experimental apparatus is a 5.5 m horizontally oriented shock tube with a 75 mm square cross-section Jacobs et al. (1995), Budzinski et al. (1994), Jacobs et al. (1993). A membrane of polypropylene separates the driver section from the driven section, and the driver section is pressurized to 20 psig. A diffuse curtain of SF_6 gas seeded with glycol droplets from a modified theatrical fog generator flows downward into the test section at a velocity less than 10 cm/s and is drawn out the bottom of the test section. The resulting curtain is perturbed using nozzles with varying varicose patterns of different wavelengths. Three Hadland SVR intensified CCD cameras (1034 × 468 pixels) are focused at various regions within the test section. The test section, pictured in Figure 1, shows the orientation of the nozzle and the three cameras.

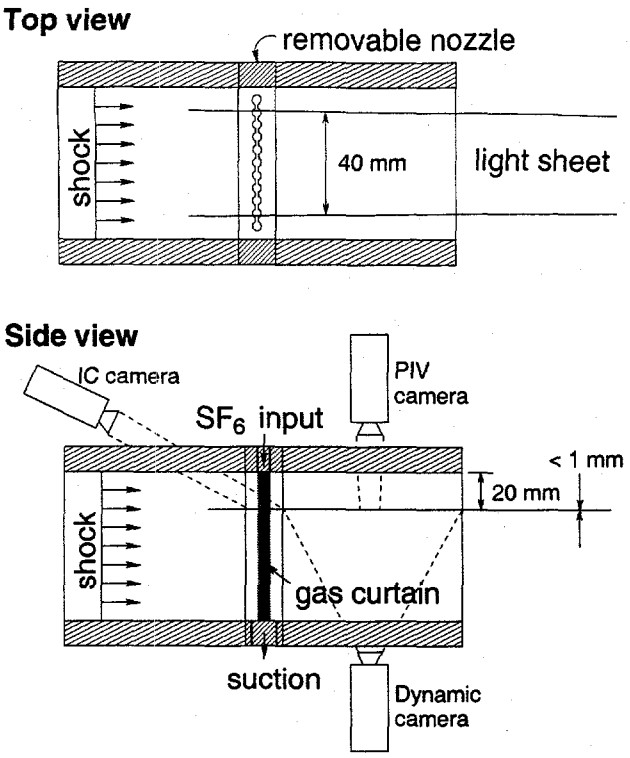

Figure 1. Schematic of the shock tube test section showing position of light sheet and three CCD cameras.

A custom-built doubled Nd:YAG laser (hereafter referred to as Laser A) was designed to be fired with up to nine pulses within a 1 ms burst. The energy per pulse averages from 3 to 5 mJ, with shot-to-shot variability. The pulses are recorded on an oscilloscope using a photodiode in order to check pulse amplitudes as well as inter-pulse times. The current setting for Laser A provides seven equally-spaced pulses at 140 μs apart. The pulses can be as closely spaced as 20 μs, however, this small time separation between pulses results in a reduction in power of the pulses. Also, smaller time separations are required to perform the PIV interrogations accurately. Consequently, a second doubled Nd:YAG laser (Laser B) from New Wave was added to the apparatus so that the single pulse from the New Wave laser could be added at any time during the pulse train of Laser A. The light sheets formed by the two lasers are focused into the test section at a distance 20 mm from the nozzle exit. This positioning allows us to examine the gas curtain in a region which has been minimally affected by the instabilities which develop near the suction outlet. Special care was taken to maintain the cross-stream intensity of the laser sheet in order to optimize the image intensity across the test section. A spherical lens sets the cross-stream width of the light sheet ($\approx$40 mm) so that it does not vary within the test section, as shown in Figure 1. A 2 m focal length cylindrical lens slowly focuses the sheet down to $\approx$1 mm vertical thickness in the test section.

Referring again to Figure 1, the fields of view of the three cameras are shown using dotted lines. The IC camera focuses only on the initial conditions, in order to provide the maximum resolution possible for use in numerical validation. The PIV camera focuses on a small region of the flow, 19 mm $\times$ 14 mm. It captures the closely-spaced pulses from both lasers, and the location of the PIV camera is moved according to the placement of the PIV pulse from Laser B. The Dynamic camera focuses on the rest of the test section and captures the multiple pulses from Laser A only. The camera is shuttered in order to remove the single pulse from Laser B.

The shock wave is initiated through a trigger of a solenoid plunger which bursts the polypropylene diaphragm and sends a Mach 1.2 normal shock down the tube. The lasers and cameras are triggered by the passage of the shock past wall-mounted pressure transducers which are mounted flush with the wall at various locations upstream of the test section.

3. Diagnostics and data processing

Seeding the flowfield with particles which track the flow is crucial for the success of the PIV technique Adrian (1991). Due to the strong accelerations present in this shock-driven flow, extensive analysis has been done to verify that the particles are tracking the SF_6 curtain. This analysis was performed in previous gas curtain experiments where PIV was not implemented Rightley et al. (1997), however we repeat some of this analysis here due to the sensitivity of PIV to particle tracking fidelity. The average diameter of the particles produced by the fog generator is $\approx 0.5\,\mu$m ETSA (1996). What must be determined is whether these particles can follow the strong accelerations to which they may be subjected throughout the experiment. We will outline several lines of reasoning which illustrate the flow tracking fidelity of the glycol droplets.

A detailed analysis of the forces which dominate the movement of heavier particles in a lighter carrier fluid was performed by Hjelmfelt & Mockros (1966) after Hinze (1959). Using this analysis, we can estimate the largest particle sizes which will be able to closely follow the fluctuations of the carrier phase. The forces which dominate the motions of the particles are Stokes' drag and inertia. For heavy particles, buoyancy, added mass and the dynamic pressure field can all be neglected. FOr this size of particle, the Weber number is small, and the particles can be considered round, except possibly for a short time during the shock compression phase. We are interested in whether or not the particle fluctuations can follow the gas fluctuta-

tions, and Hjelmfelt and Mockros estimated this by rewriting the velocities of the particles and gas in frequency space, such that:

$$v_p(\omega) = \int_{-\infty}^{\infty} \vec{u_p} e^{-i\omega t} d\omega \text{ and } v_g(\omega) = \int_{-\infty}^{\infty} \vec{u_g} e^{-i\omega t} d\omega. \quad (1)$$

This formulation introduces a characteristic frequency of the flow, ω, and the p and g subscripts denote particles and gas, respectively. Using the known force balance, the ratio of the fluctuations can be written in the form (Hjelmfelt & Mockros (1966)):

$$\frac{|\vec{v_p}|^2}{|\vec{v_g}|^2} = \frac{(18St^2/s)^2}{(18St^2/s)^2 + 1}, \quad (2)$$

where

$$St = \sqrt{\frac{\nu_g}{\omega d^2}} \text{ and } s = \frac{\rho_p}{\rho_g}. \quad (3)$$

By requiring that the energy spectrum of the fluctuations of the particles be within 1% of the spectrum of the fluctuations of the gas, we apply a very strong constraint on the limit of acceptable particle diameters. One can estimate the early-time frequencies to which the particles are subjected by considering the width of the gas curtain and the shock speed to give us an estimate of the characteristic frequency of the flow. For a shock speed of 400 m/s and a 6 mm curtain width, the 67 kHz frequency can be followed by particles which are at most 0.8 μm in diameter. At late times, there are several ways to estimate the flow frequencies. Using the spatial resolution of the PIV, which is 0.5 mm, and the approximate maximum fluctuating velocity component in the flow of 10 m/s, the frequency is only 20 kHz, and the particles need only be less than 1.5 μm. Using a more conservative estimate, the smallest time separation between PIV images is 10 μs, or a frequency of 100 kHz. This requires that the particles be at most 0.7 μm in diameter. Even at this most stringent requirement, the fog particles are still able to follow the flow.

Another, more direct check of whether or not the particles are following the flow is to compare the images of direct Rayleigh scattering of SF_6 from early experiments (Budzinski et al. (1994)) to images of light scattered from the fog particles. Figure 2 shows an image from the experiments of Budzinski et al. (1994). The image is formed by the direct Rayleigh scattering of SF_6 using a laser sheet, and the images are of the initial conditions and at $t = 450\,\mu$s. By choosing a recent shot from the new experimental configuration, which uses glycol droplets to seed the SF_6 curtain and a pulsed laser sheet for imaging, a comparison between the two imaging techniques can be made and the fidelity of the particle tracking confirmed. The lower image in Figure 2 is an image of light scattering by the fog using the pulsed light sheet. Upon initial visual inspection, the fog particles appear to track the SF_6 identically.

A more detailed examination can be made by looking at the intensity profiles through cross-cuts of similar flow features. Figure 2 shows white lines where the cross-cuts were sampled. No smoothing of the data was done. Figure 3 illustrates the profiles of pixel intensity through the initial and downstream conditions. All of the pixel intensities are normalized, and the spatial distance is normalized with the wavelength of the initial perturbation. The comparison between the initial conditions is excellent. The initial conditions also show the diffuse nature of the curtain, and the fact that there seems to be no difference between the diffusivity of the SF_6 curtain and the fog droplets. At the later time, the comparison was made between the most symmetric mushroom structures. Again, the evidence indicates that the glycol droplets are following the SF_6. From this direct evidence, we are confident that accurate velocity information about the gas curtain can be ascertained through the use of the fog as a tracer.

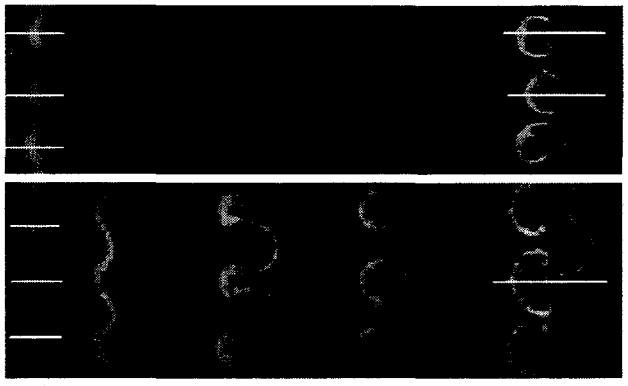

Figure 2. Direct Rayleigh scattering from SF_6 at $t = 0$ and 450μs (top), and scattering from fog and SF_6 at $t = 0, 60, 200, 340$ and 480μs (bottom). White lines indicate where pixel intensity samples were taken.

4. Observations

The following observations are a small sample of the data which has been collected so far, and they are intended to serve as an illustration of the capabilities of the diagnostics as well as proof of the feasibility and accuracy of the implementation of PIV. One of the primary reasons for implementing PIV in this experiment is to improve the quality of information available for validation of numerical simulations. With this goal in mind, we will provide an example of the qualitative and quantitative information which can be obtained from just a small amount of velocity information. The ultimate goal will be to provide much more extensive

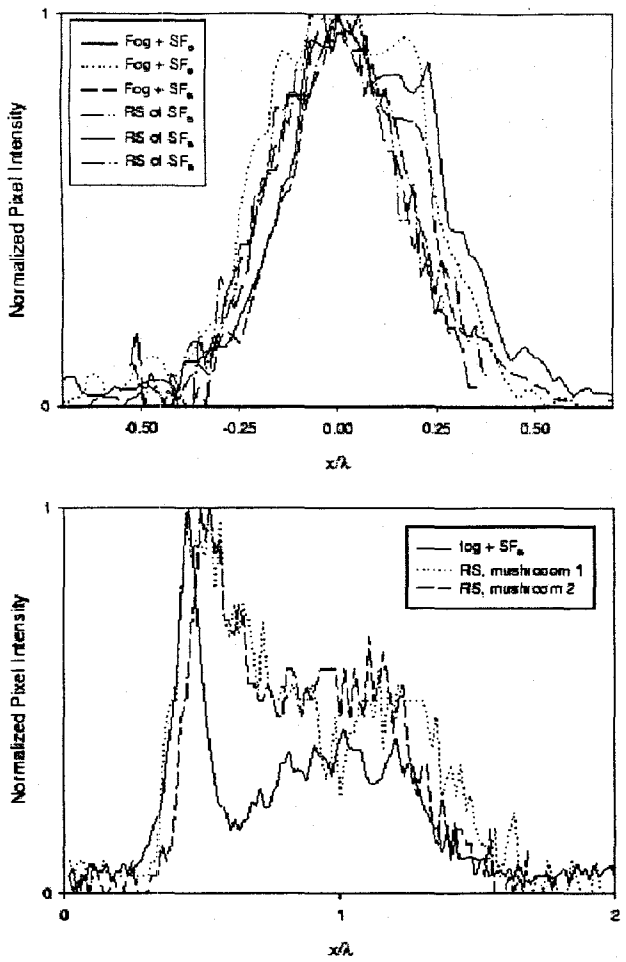

Figure 3. Comparison of normalized pixel intensities for initial conditions (left) and at late time. Samples are taken from labelled lines in Figure 2.

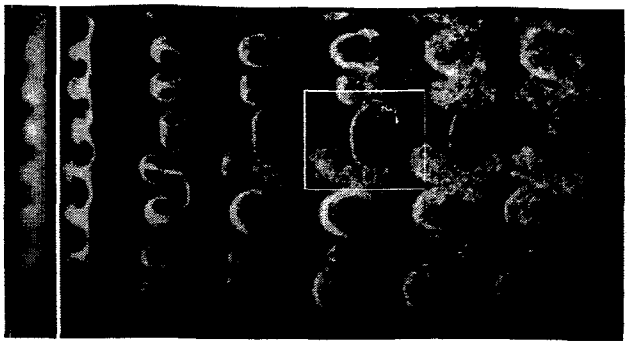

Figure 4. Case 1. Initial ($t = 0$) and dynamic ($t = 50, 190, 330, 470, 610, 750\,\mu s$) conditions for single mode nozzle, as viewed by the IC and Dynamic cameras. White box indicates field of view of PIV camera.

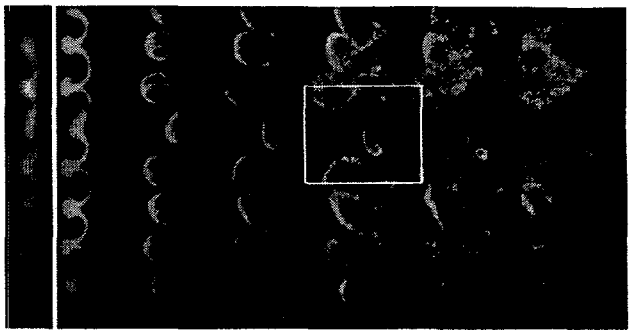

Figure 5. Case 2. Initial ($t = 0$) and dynamic ($t = 54, 194, 334, 474, 614, 754\,\mu s$) conditions for single mode nozzle.

statistical information for code validation efforts.

Figures 4 and 5 are two examples of the complete range of initial conditions and dynamic images which are captured in each experimental shot. The spatial resolution of the images is 0.1 mm/pixel. In these shots, the single mode nozzle (one wavelength, one amplitude) was used, and these images were selected due to their similar dynamic evolutions, including the stretched mushrooms caused by slightly lower amplitude perturbations in one location along the initial conditions. These images also appear similar when an integral estimate of the growth of the mixing region is made.

Through the use of quantitative measures, we would like to be able to compare these two shots and determine how they are similar or different. It is for this purpose the the PIV camera is focused on a small region of the gas curtain. Figure 6 shows the two regions from Figures 4 and 5. The figures show the two laser pulses which illuminate the flow, with a time separation of $10.4\,\mu s$. The time separation between PIV pulses (pulse from Laser B and nearest pulse from Laser A) was carefully optimized, weighing the need to accurately determine both the freestream velocity (100 m/s) and the fluctuating velocity (10 m/s). The time separation was made large enough to resolve (over at least five pixels) the fluctuating velocities, but it was kept small enough to minimize the loss in spatial resolution caused by the particles travelling quickly downstream between pulses. Optimally, this inter-pulse time for PIV was $10\,\mu s \leq \Delta t < 20\,\mu s$ based on a spatial resolution of $\approx 15\,\mu$m/pixel.

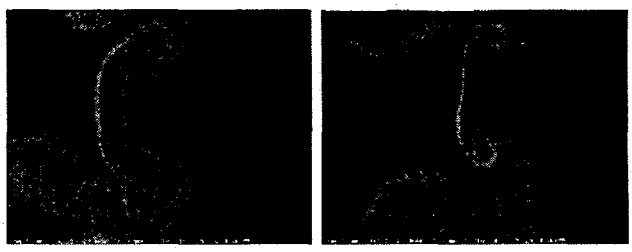

Figure 6. Closeups of regions for PIV, Case 1 (left) and Case 2, both captured using the PIV camera.

These images were interrogated using VISIFLOW software AEA Technology (1997). Due to the particle

distribution at this time in the flow evolution, interrogation box sizes of 64 pixels square were used to search for particle pairs. A technique of single frame cross-correlation was used AEA Technology (1997), and the second box was displaced downstream from the first using an estimated freestream velocity of 100 m/s. The resulting velocity fields are shown in Figures 7 and 8, superimposed upon the original images.

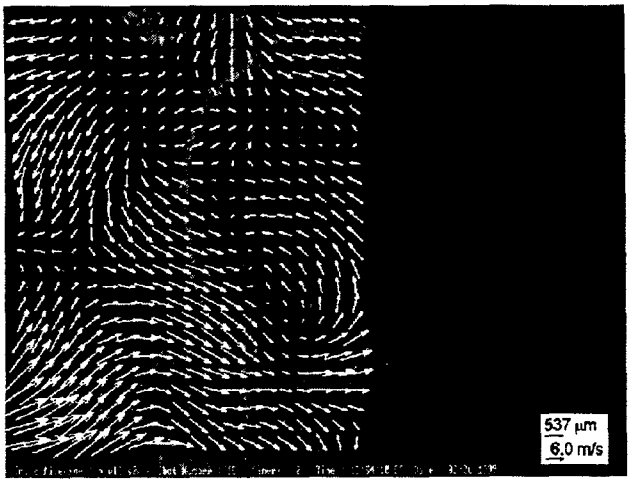

Figure 7. Case 1. Interrogated velocity field with mean velocity (97 m/s) subtracted. Invalidated vectors have been removed.

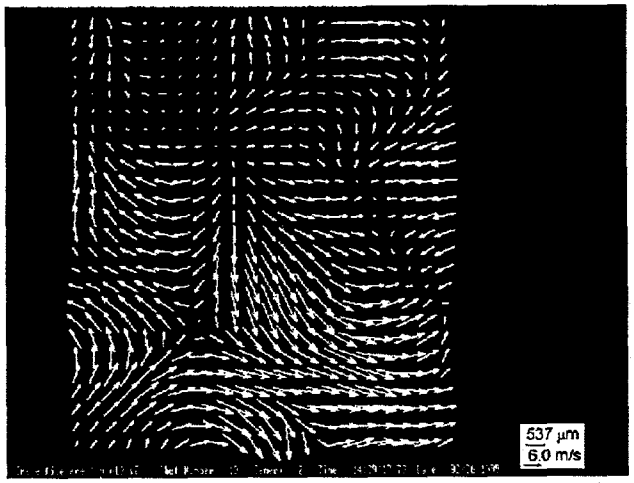

Figure 8. Case 2. Interrogated velocity field with mean velocity (97 m/s) subtracted.

In Figures 7 and 8, the mean velocity, which in both cases is 97 m/s, has been subtracted. The velocity vectors have been smoothed using a Gaussian 5×5 filter to reduce noise. Also, the vectors have been validated using a control-volume (CV) approach to check that the continuity equation is satisfied. In each picture, the dark regions which appear to have no particles actually have a very low number of particles, usually 1-2 pairs per interrogation region. While this is not enough pairs to get an accurate reading of the fluctuating component of velocity, the freestream velocity was recovered. When checking continuity, we imposed strict conditions upon the difference between inflow and outflow of the CV. For the freestream velocities, the difference was less than 0.04%, and for the fluctuating velocities, the difference was less than 5% for both cases for the regions shown in the figures.

The instantaneous velocity fields are able to reconstruct the visible large scale features of the images, including the rollup of fluid behind the elongated mushrooms. Also visible are the nearby mushrooms at the top and bottom edges of the pictures, which induce strong velocities with localized curvature of the velocity vectors. More information can be determined from these validated velocity fields by calculating vorticity and other derivative quantities.

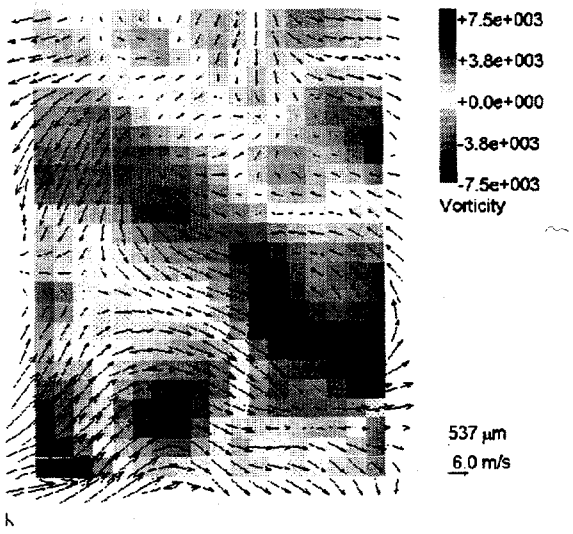

Figure 9. Case 1. Velocity and vorticity fields.

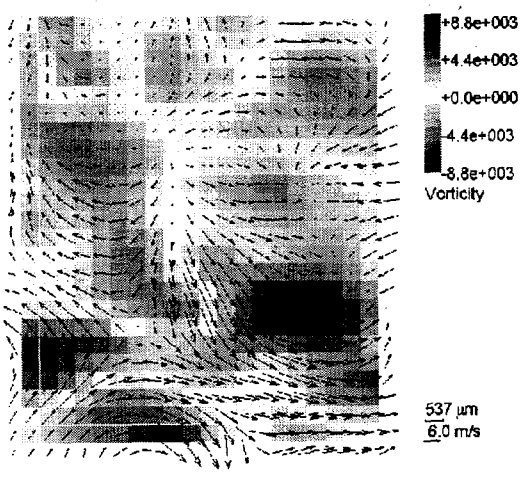

Figure 10. Case 2. Velocity and vorticity fields.

Figures 9 and 10 show the ω_z component of vorticity overlaid on the velocity fields. We can confirm the large-scale coherent vortex structures in both cases. For each case, the positive and negative vortices behind the elongated mushrooms are visible and of similar magnitudes. Also visible are the vortex structures with negative vorticity in the lower part of each figure. What these images help to highlight are the different relative positions of the vortex patches in the two different shots. Although the vortices of the primary elongated mushrooms are in similar positions, the surrounding vortices are positioned differently. In Case 1, Figure 9 shows a negative vortex almost directly upstream of the positive vortex patch from the elongated mushroom. Figure 10 shows that the negative vortex is still laterally displaced from the positive end of the elongated structure, although it is also upstream of that structure. These features were not initially obvious differences identified in the examination of the dynamic images of Figures 4 and 5. Through the accumulation of data sets containing multiple PIV and imaging, statistical information can be gathered and used to validate numerical simulations of the Richtmyer-Meshkov instability.

5. Conclusions

We have shown, through two examples, the ability of PIV to accurately reproduce velocity fields and large-scale vorticity information in the gas curtain experiment. This technique, although not new in the fluids community, has not been previously used to study the high-speed evolution of this shock-accelerated instability. The design of a customized, burst mode Nd:YAG laser, used in conjuction with a commercial pulsed laser, was necessary for the implementation of simultaneous imaging and PIV diagnostics. Two CCD cameras allow us to image high resolution initial conditions and the entire dynamic event. A third CCD camera allows us the high spatial resolution necessary to acquire PIV information by resolving the small tracking particles. The important issue of fog particle tracking fidelity has been readdressed in light of the concerns posed by the use of PIV, and we are confident that the fog droplets are following the velocity fluctuations of the flow at both early and late times.

Acknowledgement. The authors would like to thank Norman Kurnit for the design and development of the burst-mode laser.

This work was supported by DOE contract W-7405-ENG-36.

References

Meshkov, E.E. 1969: Instability of the interface of two gases accelerated by a shock wave. Izv. Akad. Nauk. SSSR Mekh. Zhidk. Gaza. 4, 151

Rightley, P.M.; Vorobieff, P.; Martin, R.; Benjamin, R.F. 1999: Experimental observations of the mixing transition in a shock-accelerated gas curtain. Phys. Fluids. 11(1), 186

Vorobieff, P.; Rightley, P.M.; Benjamin, R.F. 1998: Power law spectra of incipient gas curtain turbulence. Phys. Rev. Lett. 81(11), 2240

Rightley, P.M.; Vorobieff, P.; Benjamin, R.F. 1997: Evolution of a shock-accelerated thin fluid layer. Phys. Fluids. 9, 1770

Jacobs, J.W.; Klein, D.L.; Jenkins, D.G.; Benjamin, R.F. 1993: Instability growth patterns of a shock-accelerated thin fluid layer. Phys. Rev. Lett. 70, 583

Budzinski, J.M.; Benjamin, R.F.; Jacobs, J.W. 1994: Influence of initial conditions on the flow patterns of a shock-accelerated thin fluid layer. Phys. Fluids. 6, 3510

Jacobs, J.W.; Jenkins, D.G.; Klein, D.L.; Benjamin, R.F. 1995: Nonlinear growth of the shock-accelerated instability of a thin fluid layer. J. Fluid Mech. 295, 23

Adrian, R.J. 1991: Particle-imaging techniques for experimental fluid mechanics. Ann. Rev. Fluid Mech. 23, 261

Entertainment Services and Technology Associates 1996. Introduction to modern atmospheric effects. New York.

Hjelmfelt, A.T.; Mockros, L.F. 1966. Motion of discrete particles in a turbulent fluid. Appl. Sci. Res. 16, 149

Hinze, J.O. 1959. Turbulence. McGraw-Hill, New York.

AEA Technology 1997. VISIFLOW System User Manual. Oxfordshire, UK.